AFRL-AFOSR-UK-TR-2023-0063

Architectured Magnetoactive Elastomers: Functionalities through Instabilities

Stephan Rudykh
Université du Luxembourg Etabl. Public
Avenue de l'Université 2
Esch-sur-Alzette, , 4365
LU

04/20/2023
Final Technical Report

DISTRIBUTION A: Distribution approved for public release.

Air Force Research Laboratory
Air Force Office of Scientific Research
European Office of Aerospace Research and Development
Unit 4515 Box 14, APO AE 09421

REPORT DOCUMENTATION PAGE

PLEASE DO NOT RETURN YOUR FORM TO THE ABOVE ORGANIZATION.

1. REPORT DATE	2. REPORT TYPE	3. DATES COVERED	
20230420	Final	START DATE 20191201	END DATE 20231130

4. TITLE AND SUBTITLE
Architectured Magnetoactive Elastomers: Functionalities through Instabilities

5a. CONTRACT NUMBER	5b. GRANT NUMBER	5c. PROGRAM ELEMENT NUMBER
	FA8655-20-1-7003	61102F
5d. PROJECT NUMBER	**5e. TASK NUMBER**	**5f. WORK UNIT NUMBER**

6. AUTHOR(S)
Stephan Rudykh

7. PERFORMING ORGANIZATION NAME(S) AND ADDRESS(ES)
Université du Luxembourg Etabl. Public
Avenue de l'Université 2
Esch-sur-Alzette 4365
LU

8. PERFORMING ORGANIZATION REPORT NUMBER

9. SPONSORING/MONITORING AGENCY NAME(S) AND ADDRESS(ES)	10. SPONSOR/MONITOR'S ACRONYM(S)	11. SPONSOR/MONITOR'S REPORT NUMBER(S)
EOARD UNIT 4515 APO AE 09421-4515	AFRL/AFOSR IOE	AFRL-AFOSR-UK-TR-2023-0063

12. DISTRIBUTION/AVAILABILITY STATEMENT
A Distribution Unlimited: PB Public Release

13. SUPPLEMENTARY NOTES

14. ABSTRACT
In summary, we have analyzed a design of magneto-mechanical metamaterial with a strain-tunable attenuation regime. The design utilizes the structural transformations induced by magnetic interactions and global deformation. The design can be further optimized through tailored architecture with engineered operating frequency range tuning. The numerical results should be verified by experimental measurements of the transmittance spectra of vibrations in the relevant frequency ranges and excitation modes.

15. SUBJECT TERMS

16. SECURITY CLASSIFICATION OF:			17. LIMITATION OF ABSTRACT	18. NUMBER OF PAGES
a. REPORT	b. ABSTRACT	c. THIS PAGE		
U	U	U	SAR	12

19a. NAME OF RESPONSIBLE PERSON	19b. PHONE NUMBER *(Include area code)*
DAVID SWANSON	785-6565

Standard Form 298 (Rev.5/2020)
Prescribed by ANSI Std. Z39.18

DISTRIBUTION A: Distribution approved for public release.

Final Project Report

European Office of Aerospace Research and Development (EOARD)

EOARD Grant # 19IOE010

Prepared by: Dr. Stephan Rudykh

We started by investigating the propagation of shear or transverse waves in magnetoactive periodic layered microstructure (as illustrated in Fig. 1) under the effect of an external magnetic field.

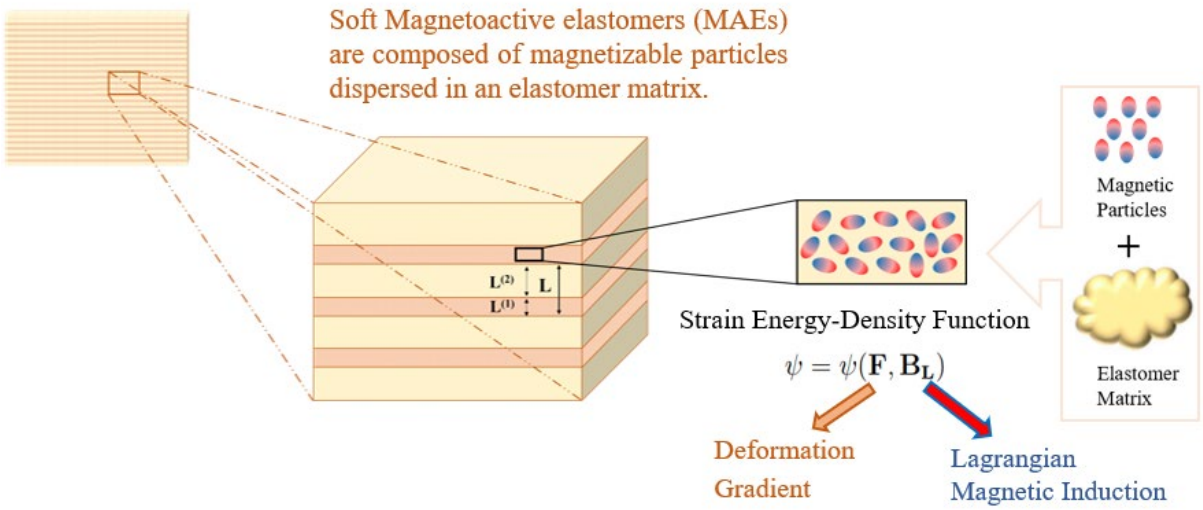

Figure 1: Schematics of the soft periodic magnetoactive laminate: each phase is considered to be homogenous at the microstructure length scales, while the phase can include small size magnetizable particles of sufficiently smaller sizes.

The layered MAEs exhibit both geometrical and material nonlinearities when subjected to a remotely applied magnetic field. The nonlinear magneto-mechanical coupling of the considered MAE phases is modeled with the help of the following total free energy density function (EDF):

$$\psi^{(\xi)}(I_1^{(\xi)},\ I_4^{(\xi)},\ I_5^{(\xi)}) = \psi_{elas}^{(\xi)}(I_1^{(\xi)}) + \frac{1}{2\mu^{(\xi)}}(\gamma_0\ I_4^{(\xi)} + \gamma_1\ I_5^{(\xi)})$$

The total EDF is a superposition of purely mechanical and magneto-mechanical terms, which are functions of the deformation gradient and magnetic induction. Note that the important ingredient

DISTRIBUTION A: Distribution approved for public release.

of including the fourth invariant (typically ignored in the MAE modeling). Our intermediate results indicate the significant influence of the term on the shear waves propagating in the MAE laminates. For the elastic part, the strain energy density function of incompressible the neo-Hookean (although other functions, such as Gent model accounting for the stiffening effects of the limiting polymer chain extensibility, are considered as well) with the elastic properties characterized by the phase initial shear moduli. To study the role of the applied magnetic field as well on the wave propagation in soft MAE laminates, we make use of the phase constitutive equations, interface jump condition for displacement and magnetic field, as well as magnetostatics equations. Next, we linearize the constitutive relations at a given point along the magneto-mechanical loading path, and solve the incremental equation of motion (superimposed on the finite deformation in the presence of an applied magnetic field):

$$\mathrm{Div}\dot{\mathbf{P}} = \rho_0 \mathbf{u}_{,tt}$$

By making use of the Floquet periodicity, and interface jump condition, we derive the dispersion relations for the infinitesimal steady-state shear waves traveling perpendicularly to the finitely deformed layers are derived:

$$\cos kl = \cos\left(\frac{\omega\, l^{(1)}}{c^{(1)}}\right)\cos\left(\frac{\omega\, l^{(2)}}{c^{(2)}}\right) - \frac{1}{2}\left(\frac{\rho^{(1)}c^{(1)}}{\rho^{(2)}c^{(2)}} + \frac{\rho^{(2)}c^{(2)}}{\rho^{(1)}c^{(1)}}\right)\sin\left(\frac{\omega\, l^{(2)}}{c^{(2)}}\right)$$

While the dispersion relation attains the classical form for the laminates, the important difference is in the expression of the phase velocities that explicitly depend on the magnetic field (even in the undeformed configuration). The velocities of the shear waves traveling normal to the layers and the band structure depend on the applied magnetic intensity and induced strains. Through the dispersion relations, we demonstrate the appearance and tunability of the shear wave band gaps with the magnetic field and material properties of the constituents. Band gaps are the frequency ranges that elastic/acoustic waves cannot propagate through the medium. The obtained results show that the **tunability of the shear wave band gaps,** even for the neo-Hookean MAE with an enriched magnetic response, **is possible** in contrast to the previous result obtained from the neo-Hookean MAE with a linear magnetic response. Together these results provide important insights into the control and manipulation of elastic waves in soft magnetoactive composites.

DISTRIBUTION A: Distribution approved for public release.

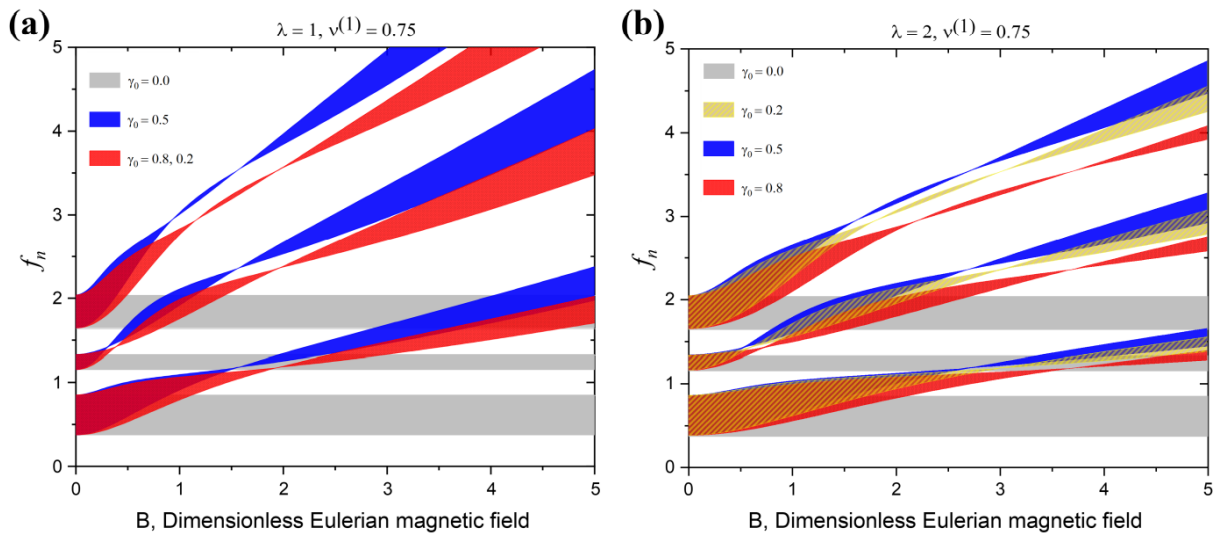

Figure 2: The first three shear waves band gaps versus the nondimensional applied Eulerian magnetic induction (a) in the undeformed state ($\lambda = 1$), and (b) in the deformed state ($\lambda = 2$) for $\gamma_0 = 0$, 0.2, 0.5, and 0.8 in the neo-Hookean MAE laminates with $\nu^{(f)} = 0.75$, $G^{(f)}/G^{(m)} = 15$, $\mu_r^{(f)}/\mu_r^{(m)} = 5$, $\rho^{(f)}/\rho^{(m)} = 1$. Frequency is normalized as $f_n = (\omega L/2\pi)\sqrt{\bar{\rho}/\bar{G}}$.

Figure 2 illustrates the dependency of the first three shear wave band gaps on the nondimensional applied Eulerian magnetic induction B, by changing the parameter γ_0. The stretch ratio in the undeformed and the deformed state are $\lambda = 1$ and $\lambda = 2$, respectively. The volume fraction of the stiffer layer is $\nu^{(f)} = 0.75$. The material properties of the neo-Hookean layered MAEs are, $G^{(f)}/G^{(m)} = 15$, $\mu_r^{(f)}/\mu_r^{(m)} = 5$, $\rho^{(f)}/\rho^{(m)} = 1$. In all figures, the horizontal gray areas represent the first three shear wave BGs when the magneto-elastic coupling parameter is $\gamma_0 = 0$. One can see that when $\gamma_0 \neq 1$, the width, shape, and position of the shear wave band gaps change by applying the magnetic induction on the MAE laminates with the neo-Hookean magnetoactive phase, which is not possible in ideal MAE laminates. Clearly, the magnetic field shifts shear wave band gaps up toward higher frequencies. Also, by increasing the magnetic induction when there is no deformation, the slope and the rate of change of thickness of shear BGs is higher than when there is an applied deformation.

DISTRIBUTION A: Distribution approved for public release.

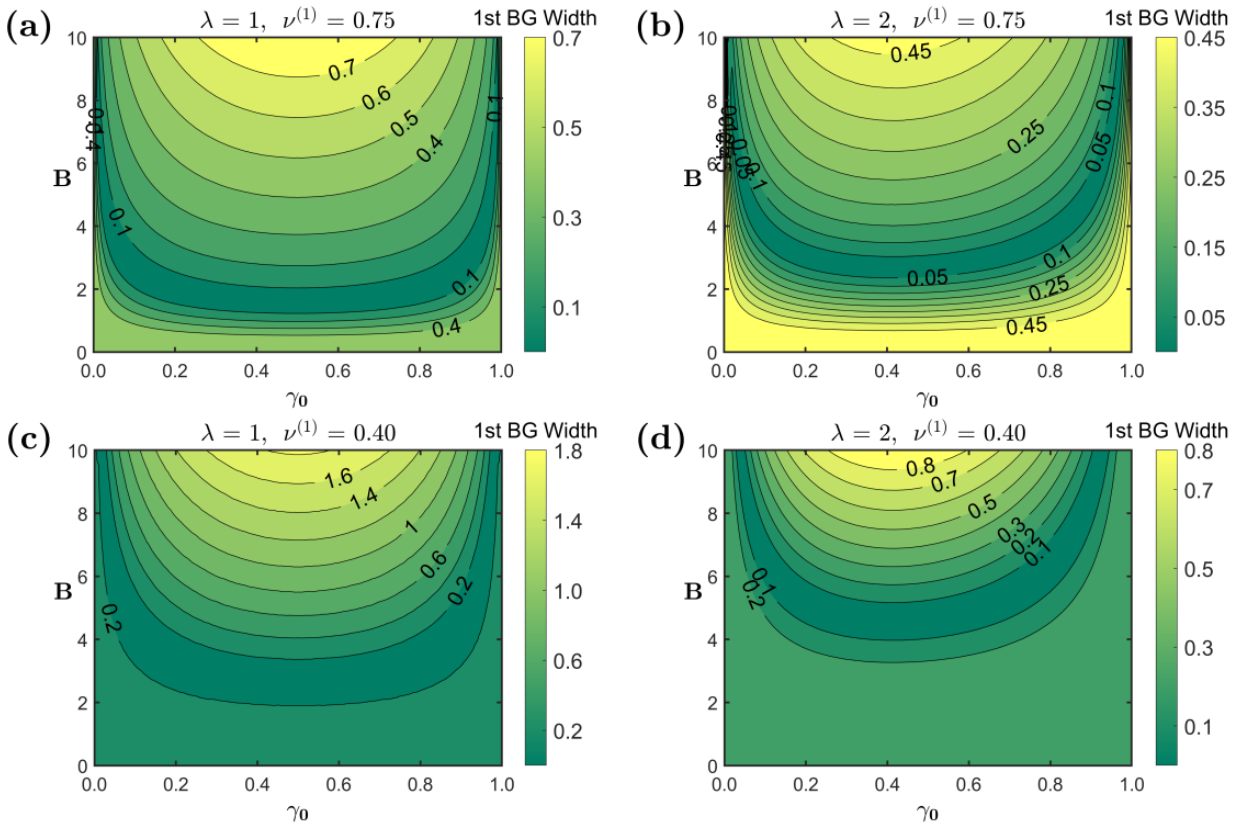

Figure 3: Thickness of the first shear waves band gaps contour map as a function of dimensionless Eulerian magnetic induction B, and I_4 coefficient, γ_0 for (a) $\lambda = 1$ and $\nu^{(f)} = 0.75$, (b) $\lambda = 2$ and $\nu^{(f)} = 0.75$, (c) $\lambda = 1$ and $\nu^{(f)} = 0.40$, (d) $\lambda = 2$ and $\nu^{(f)} = 0.40$ in neo-Hookean MAE laminates with $G^{(f)}/G^{(m)} = 15$, $\mu_r^{(f)}/\mu_r^{(m)} = 5$, $\rho^{(f)}/\rho^{(m)} = 1$.

Figure 3 depicts the dependency of the thickness of the first shear wave band gaps on the nondimensional applied Eulerian magnetic induction B and parameter γ_0, and by the change of volume fractions of the stiffer layer. The stretch ratio in the undeformed and the deformed state are $\lambda = 1$ and $\lambda = 2$, respectively. In Figure 3, one can see that wider shear band gaps occur at a lower volume fraction of stiff layer and higher nondimensional Eulerian magnetic induction: Fig 3(c). With increasing the magnetic field, the wider bandgaps happen around the vertical axis crossing from $\gamma_0 = 0.5$. The elongation in the direction of the magnetic field ($\lambda = 2$) makes the magnetic field less effective (slower) for adjusting the band gaps. In other words, at large stretch ratios, a higher magnetic field is required to achieve the same result.

DISTRIBUTION A: Distribution approved for public release.

Influence of magnetic saturation:

Next, we study the elastic wave propagation in periodic layered composites with magnetoactive phases exhibiting *magnetic saturation* behavior. The layered material is schematically shown in Fig. 1. The corresponding total energy-density functions (EDF) for soft magnetoelastic laminates with magnetic saturation and nonlinear magnetic responses are

$$\psi^*(\mathbf{F},\mathbf{B}) = \psi_{elas}(\mathbf{F}) + \rho\Psi^*_{m,\ Lang}(\mathbf{B}) + \frac{1}{2\ \mu_0}\ \mathbf{B}\cdot\ \mathbf{B}$$

where **F** is the deformation gradient, **B** is the Eulerian magnetic induction, μ_0 is the (initial) magnetic permeability of vacuum, and ψ_{elas} is the mechanical energy density function. In particular, we consider soft magnetoactive laminates with neo-Hookean or Gent magnetoactive constituents. The magnetic energy function can be modeled with the *Langevin* function as

$$\rho\Psi^*_{m,\ Lang}(\mathbf{B}) = -\frac{\mu_0\ m_s^2}{3\chi_B}\left[\ln\left(\sinh\left[\frac{3\chi_B\ |\mathbf{B}|}{\mu_0\ m_s}\right]\right) - \ln\left(\frac{3\chi_B|\mathbf{B}|}{\mu_0\ m_s}\right)\right]$$

where χ_B is the relative susceptibility (or the linearized magnetic susceptibility), |B| is the absolute value of the magnetic induction vector, and m_s (Am^{-1}) is the saturation magnetization.

we derive the closed-form dispersion relations for the infinitesimal steady-state shear waves traveling perpendicularly to the finitely deformed layers. While the form of the dispersion relation is similar to the one derived for the ideal MAE laminates, the bandgaps exhibit a different tunability with the magnetic field and by magnetically induced deformation. This is due to the difference in the phase velocities of the shear waves in the MAE phases with the magnetic saturation behavior. The analysis shows that the bandgap tunability significantly depends on the ratio of shear moduli of contrasts, relative permeability ratio, *magnetic saturation*, and volume fractions of the MAE layers at a constant magnetic field.

DISTRIBUTION A: Distribution approved for public release.

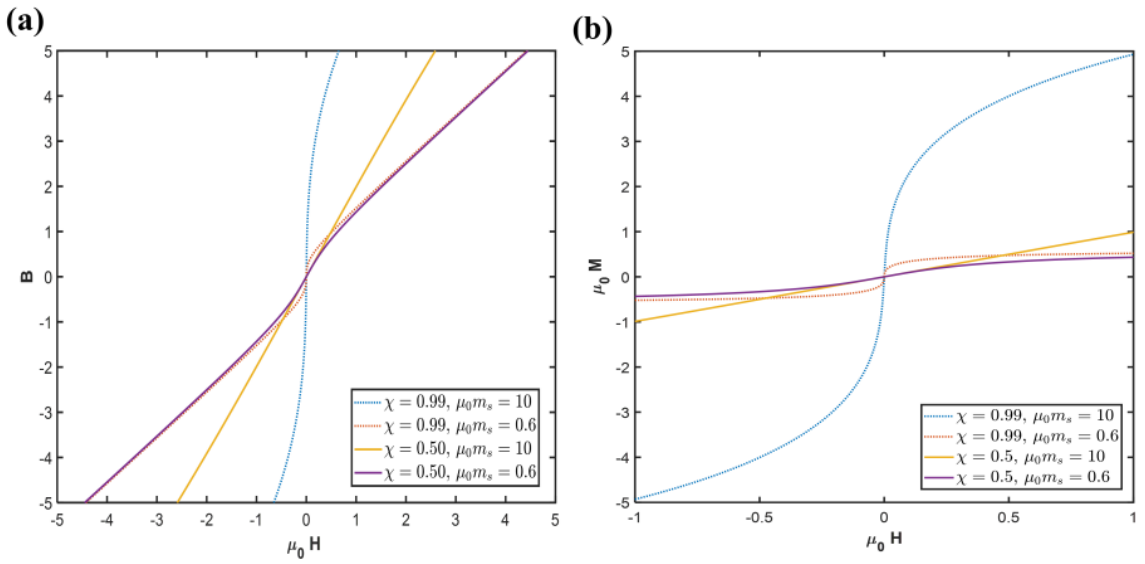

Figure 4: The magnetic behavior of the magnetoactive layers with saturation magnetization modeled the Langevin function (a) magnetic induction and (b) magnetization versus the magnetic field with the magnetic susceptibility of χ = 0.50 and 0.99, and the magnetic saturation of $\mu_0 m_s$ = 0.6 T and $\mu_0 m_s$ = 10 T.

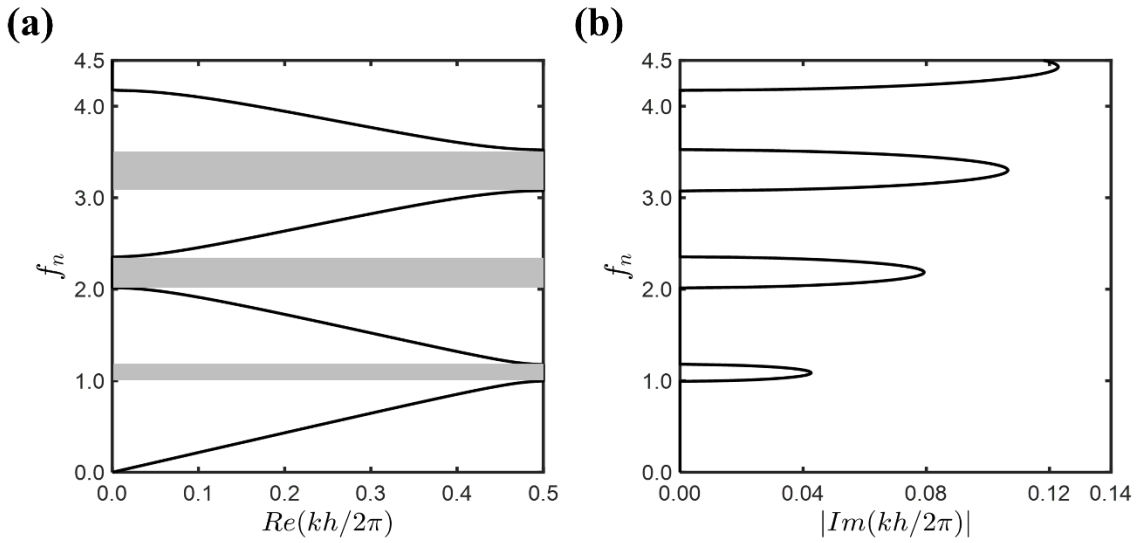

Figure 5: Dispersion diagrams for (a) real part and (b) imaginary part for shear waves in Gent MAE laminates with J_m = 0.2, $\nu^{(1)}$ = 0.2, $m_s^{(1)}/m_s^{(2)}$ = 12.5, $\mu_0 m_s^{(2)}$ = 0.4 T, $G^{(1)}/G^{(2)} = \mu_r^{(1)}/\mu_r^{(2)}$ = 5, $\mu_r^{(2)}$ = 5 and $G^{(2)}$ = 1 MPa. The dimensionless Eulerian magnetic induction of B = 2 is applied to the laminate. The shaded rectangles refer to the shear wave band gaps. Frequency is normalized as $f_n = (\omega L/2\pi)\sqrt{\bar{\rho}/\bar{G}}$.

Figure 5 illustrates a dispersion relation for the MAE laminate with Gent phases having J_m = 0.2, $\nu^{(1)}$ = 0.2, $m_s^{(1)}/m_s^{(2)}$ = 12.5, $\mu_0 m_s^{(2)}$ = 0.4 T, $G^{(1)}/G^{(2)} = \mu_r^{(1)}/\mu_r^{(2)}$ = 5, and $\rho^{(1)}/\rho^{(2)}$ = 1. The

DISTRIBUTION A: Distribution approved for public release.

composite is subjected to the dimensionless Lagrangian magnetic induction of magnitude $B_L = 1.6$, with the corresponding induced stretch being $\lambda = 1.25$. The dispersion relation has several frequency ranges where shear waves are not allowed to propagate, i.e., band gaps, denoted by the shaded areas. The lowest bandgap is induced around the mid-gap Bragg frequency that can be evaluated directly from the diagram in Fig. 5 (a) as the intersection of a tangent to the fundamental mode around the origin and the Brillouin zone boundary at $Re(kl/2\pi) = 0.5$. This fact, together with the smooth variations of the imaginary parts of the dispersion bands (Fig. 5(b)), points out the Bragg scattering origin of the bandgap mechanism.

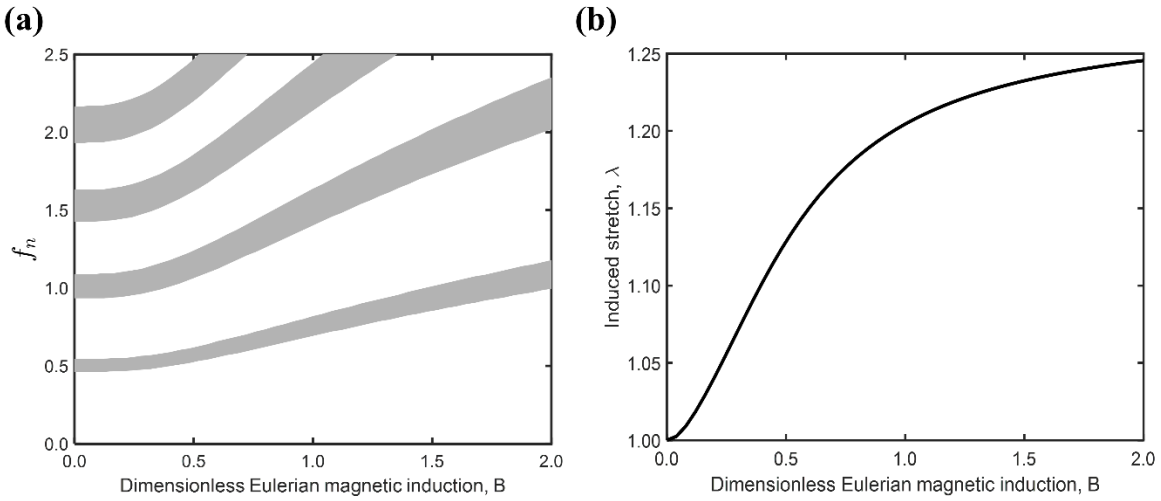

Figure 6: The dependency of (a) the first fourth shear wave band gaps and (b) induced stretch versus the dimensionless applied Eulerian magnetic induction in MAE Gent laminate with $J_m = 0.2$, $\nu^{(1)} = 0.2$, $m_s^{(1)}/m_s^{(2)} = 12.5$, $\mu_0 m_s^{(2)} = 0.4$ T, $G^{(1)}/G^{(2)} = \mu_r{}^{(1)}/\mu_r{}^{(2)} = 5$, $\mu_r^{(2)} = 5$ and $G^{(2)} = 1$ MPa. Frequency is normalized as $f_n = (\omega L/2\pi)\sqrt{\bar{\rho}/\bar{G}}$.

Figure 6 illustrates the dependency of the first to fourth shear wave bandgaps (Fig. 6(a)) and induced stretch (Fig. 6(b)) on the dimensionless Eulerian magnetic induction B applied perpendicularly to the layers in the MAE laminates with Gent magnetoelastic phases. Clearly, the magnetic field widens and shifts shear wave band gaps up towards higher frequencies. For instance, the applied $B = 2$ to the laminate shifts the lower boundary of the first shear bandgap from $f_n = 0.463$ up to 0.997 and widens it from $\Delta f_n = 0.08$ up to = 0.18.

DISTRIBUTION A: Distribution approved for public release.

Mechanically tunable material with internal magnets and without external magnetic field

Finally, we study a design of magneto-mechanical metamaterial that offers tunable frequency filtering without applying an external magnetic field. We consider a design with programmed non-uniform deformation in the materials, which is induced by the graded architected design and the magnetic interaction between the inclusions. Through our simulation, we show the induction of vibration attenuation frequency ranges via applied deformation, leading to the transformation in the propagation of waves in this metamaterial. We illustrate the numerical results by the transmittance spectra calculated at different levels of applied deformations (from undeformed to finite strain levels).

Frequency domain analysis

In this study, we investigate the propagation of pressure waves traveling from top to bottom in the magneto-mechanical metamaterial. We perform the frequency domain analysis on the finitely deformed state to obtain the transmittance spectrum. To perform the analysis, we apply periodic boundary conditions on the right and left boundaries. On the pre-deformed metamaterial, a harmonic perturbation is imposed on the top boundary with an amplitude A_{in}. The induced harmonic response at the bottom boundary is captured, and the transmittance spectrum is computed as the ratio between the output and input displacements, defined as $20\log_{10}\left||A_{out}(\omega)/A_{in}|\right|$, where ω is the frequency.

Transmittance spectrum

Figure 7 shows the transmittance spectra for pressure waves traveling from the top to bottom boundary. The results are presented for the undeformed state, $\varepsilon = 0$ (a), and deformed states at strains: $\varepsilon = 0.064$ (b), $\varepsilon = 0.124$ (c), and $\varepsilon = 0.161$ (d).

In the undeformed state $\varepsilon = 0$, we observe that the metamaterial has positive transmittance for almost all the frequency values in the considered range – 1 to 300 Hz (see Fig. 7a). This means that it allows the wave of most of the frequencies to pass through. At compression level $\varepsilon = 0.064$, where the center row of void collapses, we observe that the transmittance curve shift below the zero line for a range of frequency at smaller values (approximately 20 to 75 Hz, see Fig. 7b).

We find that in the metamaterial with two collapsed rows, at $\varepsilon = 0.124$, the transmittance curve further shifts down giving rise to multiple bandgaps (see Fig. 7c). Further, with the third collapse

DISTRIBUTION A: Distribution approved for public release.

at $\varepsilon = 0.161$, the metamaterial exhibits a highly lossy response, not only at smaller frequencies but also at higher values (see Fig. 7d). Note that this drastic change in the acoustic behavior of the metamaterial is achieved only through applied deformation (compare Fig. 7a and d). Therefore, it can be reversed by reinstating the initial microstructure by changing the compression level.

We note that the possible loss factors of the soft matter are not considered, and may be important for further validation in experiments. This may require characterization of the soft matrix material behavior in the relevant frequency ranges (such as Dynamic Mechanical Analysis), and incorporating the frequency dependence in the numerical calculations. Also, the deformation is assumed to be applied quasi-statically (corresponding to low-frequency ranges).

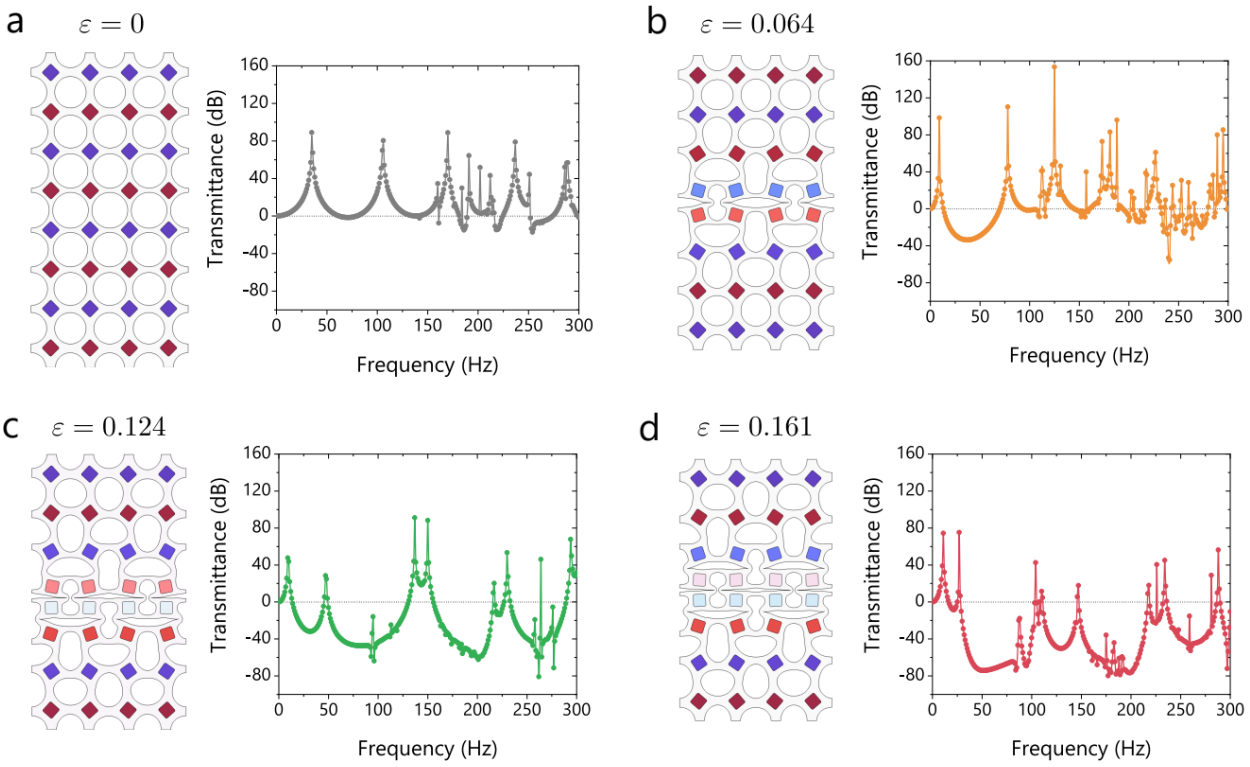

Figure 7. Transmittance spectra at strain levels, showing the state of the material (from undeformed to deformed at various strain levels: **a.** $\varepsilon = 0$, **b.** $\varepsilon = 0.064$, **c.** $\varepsilon = 0.124$, and **d.** $\varepsilon = 0.161$. Each sub-figure includes the corresponding transmittance spectrum of the deformed state.

DISTRIBUTION A: Distribution approved for public release.

To investigate the mechanism leading to the formation of bandgaps, we study the eigenmodes at strain $\varepsilon = 0.161$. Figure 8 shows the eigenmodes at low-range and high-range frequencies, namely, $f = 40$ Hz and $f = 250$ Hz. Note that at both these frequencies there is a negative transmission. The color on the eigenmodes shows the vertical displacement as per the color bar on the right.

From the color distribution in the eigenmode at $f = 40$ Hz, we can identify three distinct regions. First, the top region is red in color. Second, the center region with collapsed voids with dark blue color. The third region is the bottom region colored in the light shade of blue corresponding to almost zero displacement. This shows that the first region acts as a single rigid body, and it moves down towards the applied perturbation at the top boundary. There is almost no deformation inside the region. The second region in the center moves up, opposite to the applied harmonic perturbation. We observe that the deformation in the eigenmode is highly localized in the beams connecting the two regions. The distribution of the displacement field observed here highlights the presence of a *local resonator*. Note that this resonator is formed because of the macro-structural changes due to the applied compression. The interaction of this local resonator with the elastic waves gives rise to the low-frequency bandgap.

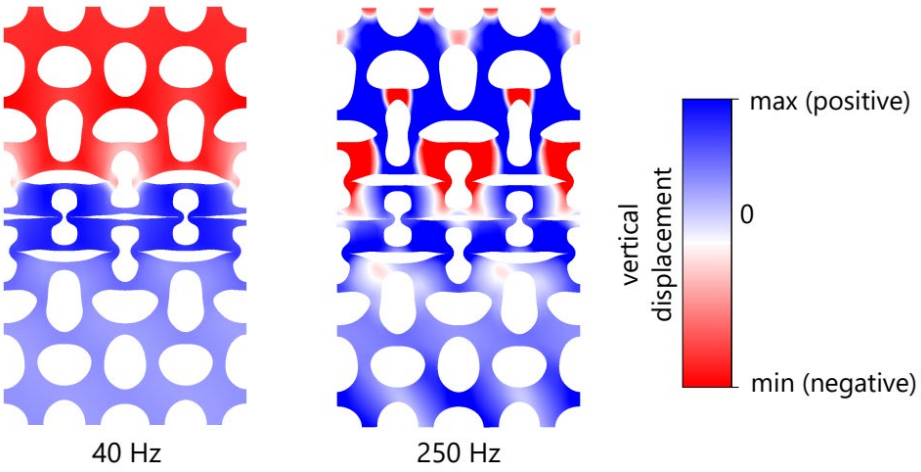

Figure 8: Eigenmodes at frequencies $f = 40$ Hz and $f = 250$ Hz at strain $\varepsilon = 0.161$. The color on the eigenmodes shows the vertical displacement as per the color bar on the right.

At $f = 250$ Hz, we observe that the displacement field is locally distributed according to the microstructure in the upper half of the metamaterial. Therefore, the existence of a bandgap at this

DISTRIBUTION A: Distribution approved for public release.

frequency can be potentially due to *Bragg scattering* at higher values of frequency. In the lower half, the displacement is close to zero (similar to 40 Hz eigenmode).

To further probe into the mechanism, in the eigenmodes at $\varepsilon = 0.161$, we analyze the vertical displacement of two magnetic inclusions in the collapsed region. The frequencies considered here lie in the bandgap regions. The two magnetic inclusions under consideration are shown in Fig. 9. These inclusions have a collapsed void between them. The rationale behind this analysis is: if there is no relative displacement between the inclusions, then it shows the occurrence of resonance, where the whole collapsed region oscillates as a single body. However, if there is relative displacement, then that represents the open-close oscillation of the voids in the collapsed region. This corresponds to the Bragg scattering phenomenon, also seen in periodic architecture with square distribution of voids.

We observe that at smaller frequency values, both the inclusions move towards the same direction with almost the same amplitude, opposite to the applied harmonic perturbation. This confirms the local resonant behavior. However, at higher frequencies (≥130 Hz), we find that the displacement of these inclusions differs. Interestingly, at $f = 250$ Hz, the inclusions move in opposite directions, highlighting the Bragg scattering phenomenon. In the intermediate range of frequency, we anticipate that the waves do not transmit potentially because of the combination of both the mechanisms.

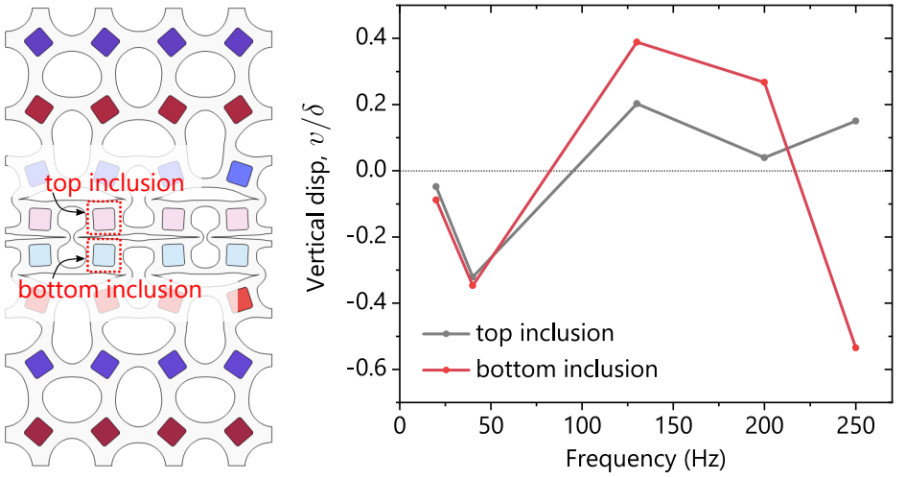

Figure 9: Vertical displacement of the two magnetic inclusions in the eigenmodes of various frequencies at strain $\varepsilon = 0.161$.

DISTRIBUTION A: Distribution approved for public release.

In summary, we have analyzed a design of magneto-mechanical metamaterial with a strain-tunable attenuation regime. The design utilizes the structural transformations induced by magnetic interactions and global deformation. The design can be further optimized through tailored architecture with engineered operating frequency range tuning. The numerical results should be verified by experimental measurements of the transmittance spectra of vibrations in the relevant frequency ranges and excitation modes.

DISTRIBUTION A: Distribution approved for public release.